ADVANCED FUNCTIONAL MATERIALS
www.afm-journal.de

Materials Views
www.MaterialsViews.com

Octupolar Films with Large Second Harmonic Generation and Electro-Optical Effects

Mi-Yun Jeong, Sophie Brasselet,* Tong-Kun Lim, and Bong Rae Cho**

Thin films that benefit from efficient octupolar molecular packing are prepared for second harmonic generation (SHG) and electro-optic (EO) applications. The films are composed of 1,3,5-tricyano-2, 4,6-tris(*p*-diethylaminostyryl)benzene (TTB) in a ploymethylmetacrylate (PMMA) matrix on aluminum/BK7 glass (Al/BK7) and polyimide/indium tin oxide (PI/ITO) substrates. Octupolar films prepared on both substrates display polycrystalline and cylindrical domains. The molecular orientation, SHG efficiencies, and EO coefficients of the crystalline domains are measured. In the cylinders, the molecular crystal planes are oriented perpendicularly to the major cylinder axis, whereas in the polycrystals, the planes are randomly oriented. While both structures exhibit high and stable SHG and EO efficiencies, the cylinders, in particular, exhibited a very large SHG, a large EO coefficient, and high thermal stability; these characteristics will be useful in second order nonlinear optical applications.

1. Introduction

Much effort has been directed to the development of octupolar nonlinear optical (NLO) materials for possible applications in second harmonic generation (SHG) and electro-optic (EO) devices.[1–5] The advantages of octupoles over more conventional dipolar molecules include their easier non-centrosymmetric arrangements, high nonlinear efficiencies due to optimum molecular packing, and a polarization-independent second harmonic response.[1b,4] A promising octupolar molecule is 1,3,5-tricyano-2, 4,6-tris(*p*-diethylaminostyryl)benzene (TTB), which not only has a large quadratic microscopic nonlinear coefficient (β_{111} = 408 × 10^{-30} esu at zero frequency[2]), but also crystallizes into a non-centrosymmetric symmetry due to the absence of a molecular net dipole moment and due to the intermolecular interactions between molecular planes. SHG measurements on such crystals in reflection have shown a record high efficiency (d_{111} = 1580 × 10^{-9}esu = 664 pm V^{-1}) at zero frequency, about 80-fold larger than that of the 3-methyl-4-nitropyridine-1-oxide (POM) crystal at zero frequency.[1] To apply these materials to integrated optical devices, it is mandatory that the thin films be fabricated with good optical quality. While thin films avoid the difficulties of growing sufficiently large bulk crystals, it is still necessary to control the surface quality and homogeneity.

Recently we reported that octupolar films, prepared by free casting the solution of TTB and poymethylmetacrylate (PMMA) in chlorobenzene on a BK7 glass plate, revealed crystalline domains having significant SHG efficiency. The nonlinear coefficient, d_{111}, of such domains was found to be on the order of 15 pm V^{-1}; however, the heterogeneous orientation patterns prevented full control of the samples' large-scale polarization response. Here, this earlier work is extended to include crystallization on different surfaces, including electrodes. Different substrates of crystallization show that it is possible to generate either polycrystalline structures or cylindrical crystals grown in a single direction. The crystalline structures, which are naturally grown without a poling process, exhibit large SHG and EO responses.

Prof. M.-Y. Jeong
Department of Physics and Research Institute of Natural Science
Gyeongsang National University
Jinju, 660-701, South Korea
E-mail: jmy97@gnu.ac.kr
Prof. S. Brasselet
Institut Fresnel, CNRS
Université Aix Marseille III
Ecole Centrale de Marseille, Domaine Univ. St Jérôme
13397 Marseille Cedex 20, France
E-mail: sophie.brasselet@fresnel.fr
Prof. T.-K. Lim
Department of Physics
Korea University
Anamdong, Seoul 136-701, South Korea
Prof. B. R. Cho
Department of Chemistry
Korea University
Anamdong, Seoul 136-701, South Korea
E-mail: chobr@korea.ac.kr

DOI: 10.1002/adfm.201102257

2. Results and Discussion

2.1. Fabrication and Linear Optical Properties of Octupolar Patterned Films

The films were prepared by depositing a solution of TTB (20 wt%) and PMMA (80 wt%) in chlorobenzene on aluminum (200 Å)/glass (BK7) plates (≈λ/10 roughness, 3 cm × 3 cm) (Al/BK7) and polyimide (SE7492, 800 Å)/indium tin oxide plates (PI/ITO, 3 cm × 3 cm). This was followed by slow evaporation.

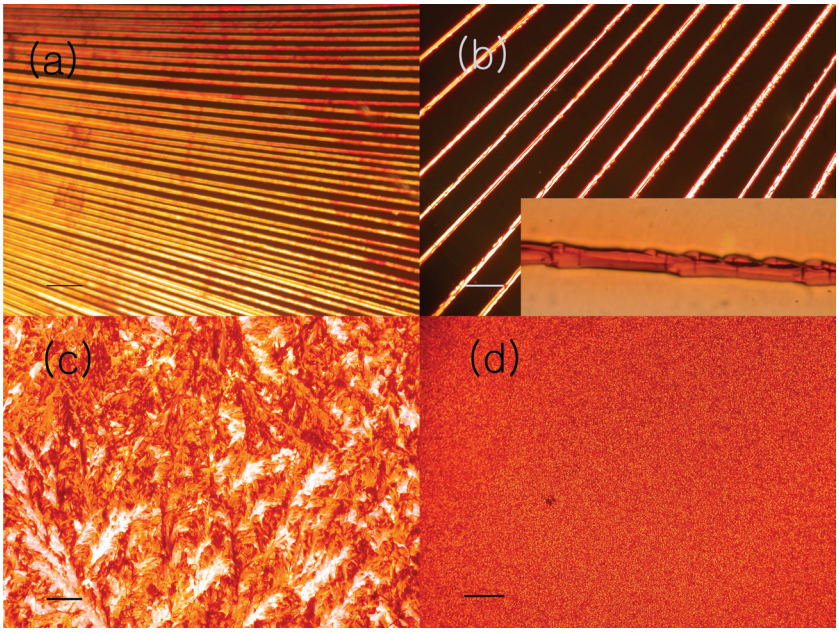

Figure 1. Polarized microscopy images of a,b) cylinders on PI/ITO, c) polycrystals on Al/BK7, and (d) PI/ITO at 100× magnification. Inset of (b) has 500× magnification. Scale bar 100 µm.

The substrates were kept at ≈9–10 °C on a vibration-free table. Three distinct patterns developed within an area on both the Al/BK7 and PI/ITO substrates (**Figure 1**): dense and sparse cylinders with ≈10–15 µm (diameter) × 6 mm (length) in a ≈6 mm domain on PI/ITO (Figure 1a,b); polycrystals in a ≈20–100 µm domain on Al/BK7 (Figure 1c); and micrometric polycrystalline features in a ≈3 mm domain on PI/ITO (Figure 1d). These patterns were developed over the entire substrate area and their directions and positions were not predictable. When the films were rotated by ≈45–50°, the bright domains turned to dark and vice versa in the polarizing microscopy images in Figure 1; this indicated a strong local birefringence in the observed domains. Therefore, the cylinders as well as the individual domains in the polycrystalline regions show local crystallinity. Such polycrystalline and cylindrical patterns were not produced when the same sample was free-casted on BK7 at ambient temperature.[1] Hence, it appears necessary that the free-casted film be maintained at a low temperature on a vibration-free table to obtain unique patterns.

The existence of crystalline domains in the free-cast films is clearly demonstrated by the X-ray diffraction (XRD) spectra (**Figure 2**a–d). The spectral peaks for the powder sample and the free-cast films coincide at $2\theta = 5.86$ and 11.72, which correspond to repeating units of 15 Å and 7.5 Å, respectively. The former is nearly identical to the length of a branch of the TTB molecule from its center, as determined by X-ray crystallography, whereas the latter is somewhat larger than the centroid separation between TTB molecules (approximately 5 Å) in the unit cell.[1] Because the unit cell consists of three molecules packed along the *c*-axis with a slight offset, the most likely structure of the crystal domain appears to be a cylinder in which the TTB planes are stacked at a distance of 7.5 Å (Figure S1 in the Supporting Information). A similar result was reported for the free-cast film on BK7.[1a]

We used birefringence experiments to assess the direction and distribution of the crystal domains in the films (Figure 2e–g). A circularly polarized 633 nm beam with a 1 mm diameter was used to illuminate a sample at normal incidence. The sample was sandwiched between two crossed polarizers that were rotated simultaneously. Polar plots represent the transmittance of the films in different regions (cylindrical-like and polycrystalline) as a function of the rotation angle. Figure 2e shows that the cylinders grown on PI/ITO have single bulk crystal domains with a strong birefringence, as revealed by an extinction every 45° of the rotation angle. The polycrystalline structure on Al/BK7 is similar but has a less clear extinction; this is characteristic of contributions from micrometric size domains that are differently oriented within the sample plane (Figure 2f). The birefringence apparent from these measurements shows that the most probable orientation of the octupoles in the crystals, both in the cylindrical and polycrystalline domains, is perpendicular to the sample plane (indeed, an octupole lying planar to the surface should lead to an isotropic response). Finally, the polycrystalline sample on PI/ITO confirms that its structure is composed of randomly oriented sub-micrometer size domains, as revealed by its complete isotropic response (Figure 2g).

We measured the absorbance spectra of the crystalline surface to investigate the optical quality of the sample (**Figure 3**). Except for the difference in amplitude due to different molecular densities, as well as a few additional features due to the Al substrate, the main molecular absorption feature is conserved and well-resolved above the scattering regardless of crystalline type (cylinder or polycrystal). This confirms the high optical quality of the samples.

2.2. Second Harmonic Generation in Octupolar Patterned Films

The second order nonlinear optical efficiency of a crystal is defined by the nonlinear susceptibility tensor, *d*, deduced from the oriented gas model.[6–8] Assuming octupolar symmetry for the TTB crystal and adopting the model developed by Zyss et al.,[1] the only non-vanishing coefficients in the (1,2,3) unit cell framework are: $d_{111} = -d_{122} = -d_{212} = -d_{221}$. To determine the 3D orientation of the crystalline structure in the domains of the studied samples and to evaluate their SHG efficiency, we first analyzed the SHG polarization responses using the configuration in Figure S2 (Supporting Information). A polarized, 1064-nm beam was used to illuminate the samples along the *Z* macroscopic direction, while the polarization angle $\Phi = (X, E^{\omega})$ of its polarization in the laboratory macroscopic frame (X, Y) plane in Figure S2a (Supporting Information) was rotated from 0 ° to 360°. The second harmonic response of the films is measured along two analyzer directions, *X* and *Y*, for which the corresponding intensities are denoted as $I^{2\omega}{}_{X,Y}(\Phi)$. We considered

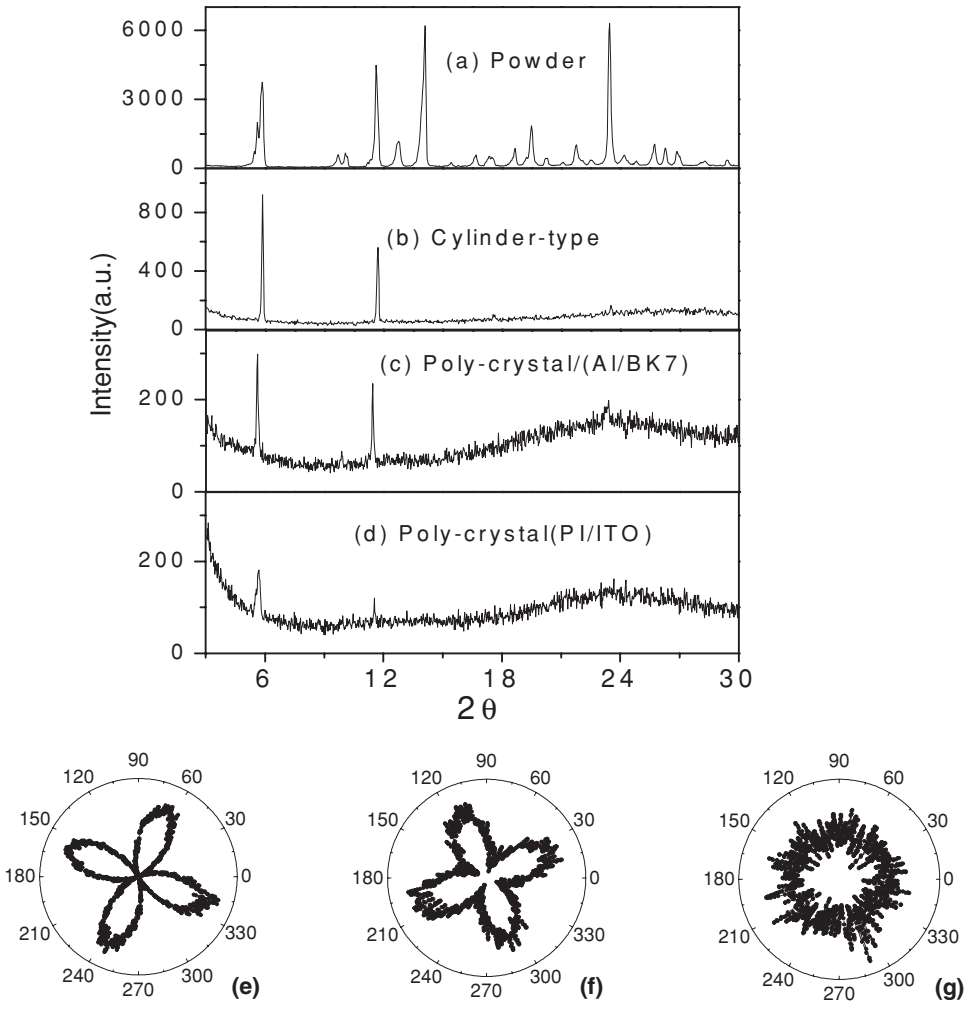

Figure 2. XRD spectra of a) TTB powder, b) cylinders on PI/ITO, c) polycrystals on Al/BK7, and d) PI/ITO. Birefringence of cylinders on e) PI/ITO, f) polycrystals on Al/BK7, and g) PI/ITO. The polar plots represent the relative transmission measured when rotating the sample in its plane between two crossed polarizers.

two different cases, in which the molecular TTB planes either lie in the (*X*,*Y*) plane (Figure S2a in the Supporting Information) or are perpendicular to this plane (Figure S2b in the Supporting Information). The corresponding intensities can be written to be proportional to

$$I^{2\omega}_{\mathrm{X,Y}}(\Phi) = \left| P^{2\omega}(\Phi) \cdot U_{\mathrm{X,Y}} \right|^2 \tag{1}$$

where $U_{\mathrm{X,Y}}$ are unit vectors in the laboratory frame, $P^{2\omega}(\Phi) = d{:}\ E^{\omega}(\Phi)E^{\omega}(\Phi)$ is the nonlinear induced dipole in the material that is formed by a tensorial product between the material nonlinear d tensor and the incident fields interaction. Considering this dipole in the unit cell crystalline frame (U_1, U_2) leads to $P^{2\omega}(\Phi, \Omega) = \sum_{I,J,K=1,2} d_{IJK} E^{\omega}_J(\Phi, \Omega) E^{\omega}_K(\Phi, \Omega) \cdot U_I$. The field components then depend on the crystal orientation defined by the Euler set of angles $\Omega = (\theta, \phi, \psi)$ depicted in Figure S1 (Supporting Information). In the situation where the TTB molecules lie in the (*X*,*Y*) plane,

$$\begin{aligned} E^{\omega}(\Phi) &= E^{\omega}[\cos\ \Phi U_1 + \sin\ \Phi U_2], \text{ and thus} \\ I^{2\omega}_X(\Phi) &= d^2_{11}(I^{\omega})^2[\cos\Phi^2 - \sin\Phi^2]^2, \\ I^{2\omega}_Y(\Phi) &= 4d^2_{11}(I^{\omega})^2\cos\Phi^2\sin\Phi^2 \end{aligned} \tag{2}$$

Equation (2) shows that the polarized response is in this case independent of the octupoles' orientation in their plane, which is to be expected in a geometry where a three-fold planar symmetry results in polarization-independent SHG. If the TTB molecules lie perpendicular to the (*X*,*Y*) plane, then

$$\begin{aligned} E^{\omega}(\Phi) &= E^{\omega}(\sin(\Phi-\phi)\sin\psi U_1 + \sin(\Phi-\phi)\cos\psi U_2), \text{ and} \\ I^{2\omega}_X(0,\Omega) &= d^2_{11}(I^{\omega})^2[\sin(\Phi-\phi)^2\sin\phi\{\sin\psi^3 - 3\sin\psi\cos\psi^2\}]^2, \\ I^{2\omega}_Y(0,\Omega) &= d^2_{11}(I^{\omega})^2[\sin(\Phi-\phi)^2\cos\phi\{\sin\psi^3 - 3\sin\psi\cos\psi^2\}]^2 \end{aligned} \tag{3}$$

Equation (3) shows that the octupoles' plane orientation can be determined by measuring the ψ-independent ratio

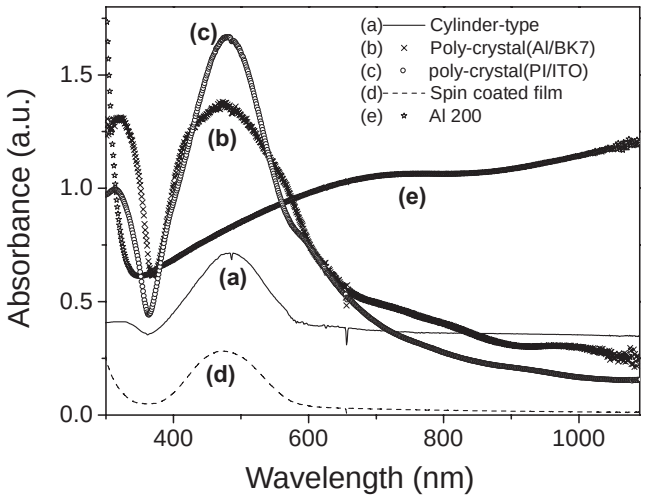

Figure 3. Absorbance spectra of cylinders on a) PI/ITO, b) polycrystals on Al/BK7, and c) PI/ITO. Spin-coated film on d) BK7 and e) Al film (200 Å) on BK7.

$I_X^{2\omega}(0,\Omega)/I_Y^{2\omega}(0,\Omega) = \tan\phi^2$ taken at the incident polarization $\Phi = 0°$.

For the SHG measurement, we employed a 1064-nm fundamental beam from a neodymium-doped yttrium aluminium garnet (Nd:YAG) laser (10 Hz, Q-switched 6.7 ns laser pulse). The focused beam, ≈150 μm in diameter, illuminated one crystal domain. For cylinders on PI/ITO, the sparse sample shown in Figure 1b was used in all experiments. The polarimetric responses of the samples are shown in a polar graph representation in **Figure 4**a–c. The polar plots for $I^{2\omega}{}_X(\Phi)$ (solid squares) and $I^{2\omega}{}_Y(\Phi)$ (open circles) for the cylinder sample exhibit two-lobe patterns and have a maximum intensity that is stronger along the *X*-axis than the *Y*-axis (Figure 4a). This indicates that $\theta(Z,U_3) = 90°$; that is, the TTB molecules lie perpendicular to the substrate plane (*X*,*Y*) (Figure S2b in the Supporting Information). Indeed, a different molecular orientation would lead to a more complex pattern due to the octupolar nature of the molecular structure. Note that the cylinders having diameters 10–15 μm are well separated from each other (Figure 1b), so that only one is present in the measurement's focus area. Therefore, the 90° difference between the two maximum angles $I^{2\omega,\max}{}_X$ (0°) and $I^{2\omega,\max}{}_Y(0°)$ and their relative intensities suggest that there are two independent molecular crystal domains in the cylinder. The directions of these domains are perpendicular to each other, and the size of the crystal whose molecular plane is parallel to the *X*–*Y* plane is much larger than the other whose molecular plane is parallel to the *X*–*Z* plane (Figure S2b in the Supporting Information). In the microscope image of the cylinder-type crystal, visible defects exhibit directions perpendicular to the cylinder main axis (Figure 1b, inset). Following this assumption, the experimental data of the polar plot agree with the theory (solid line) given by Equation (3).

The $I^{2\omega}{}_X(\Phi)$ and $I^{2\omega}{}_Y(\Phi)$ polar plots for the polycrystals on PI/ITO show an isotropic feature pattern with $I^{2\omega}{}_X(\Phi) \approx I_Y{}^{2\omega}(\Phi)$, which is the signature of a complete depolarization process (Figure 4b). Based on the microscope image (Figure 1d) and the birefringence data (Figure 2g), we conclude that microsized crystal domains are randomly oriented on the substrate. Note that the macroscopic sample structure of the polycrystal is isotropic, which is inconsistent with a coherent SHG emission. Thus, the SHG emission is incoherent in nature and each domain emits sufficient SHG intensity that adds to its randomly oriented neighbors.

The $I^{2\omega}{}_X(\Phi)$ and $I^{2\omega}{}_Y(\Phi)$ polar plot for the polycrystal film grown on Al/BK7 shows feature patterns corresponding to a nearly isotropic distribution with respect to the incident polarization angle Φ. Since $I_X{}^{2\omega}(\Phi) \geq I_Y{}^{2\omega}(\Phi)$, this indicates an incomplete depolarization. This polarization response likely originates from the presence of larger and heterogeneous crystalline domains in this structure (Figure 4c, $I^{2\omega}{}_X(\Phi)$ (open squares) and $I^{2\omega}{}_Y(\Phi)$ (solid circles)). Thus, the incoherent summation occurs over a less randomized population of domains than in the previous case. The same film illuminated with a 2 mm focal spot gave similar results in polarization (Figure S3a in the Supporting Information), which confirms that the averaged orientation process occurs for any spatial scale above 150 μm (Figure 4). Moreover, the SHG signal intensity is surprisingly enhanced more than 10-fold compared to that of the polycrystal grown on PI/ITO. When compared with the SHG intensity value of a *Y*-cut quartz crystal at normal incidence (Figure S3b in the Supporting Information), the SHG intensity $I^{2\omega}{}_X(\Phi = 0°) + I_Y{}^{2\omega}(\Phi = 0°)$ (Figure 4c, open stars) from the Al/BK7 sample is 140 ± 30 times larger than that of quartz.

The more efficient SHG response of the polycrystal on the Al/BK7 structure compared with the PI/ITO structure can be attributed to two factors. First, the larger crystalline domains on Al/BK7 allow a more efficient and coherent build-up of the signal within an individual domain of the polycrystalline structure. Second, the metallic substrate may have contributed to the enhanced SHG response. Since we used a sufficiently weak fundamental beam intensity for both samples to avoid damage, the SHG signal did not decrease during the measurement for several hours. Moreover, the two polycrystal films were prepared using the same concentration of TTB/PMMA solution and are similar in thickness (1.0 μm for Al/BK7 vs. 1.4 μm for PI/ITO). Their only major difference is the substrate, which implies that the observed enhancement on the Al/BK7 substrate may originate from its metallic nature. Due to their unique properties, metallic thin films (Al, Au, Ag) exhibit plasmon resonances that can considerably enhance optical properties such as absorption and nonlinear polarization (vide infra).[9–11]

SHG arising from a non-centrosymmetric medium on a metal thin film is expected to be proportional to the enhanced factor $|L^2(\omega)L(2\omega)|^2$, where the local field factor *L* contributes to the effect at both frequencies ω and 2ω. This SHG enhancement effect has been observed on nonlinear organic Langmuir–Blodgett films deposited on thin Al films,[12,13] and a similar effect is expected for polycrystalline films on the Al/BK7 substrate. In the presence of this enhancement, we expect the total intensity to originate from several contributions, $I^{2\omega} = I^{2\omega}{}_{\text{S-SHG}} + I_{\text{SHG}}{}^{2\omega} + I^{2\omega}{}_{\text{INT}}$. Here, $I^{2\omega}{}_{\text{S-SHG}}$, $I^{2\omega}{}_{\text{SHG}}$, and $I^{2\omega}{}_{\text{INT}}$ are the surface SHG arising from the Al surface, SHG arising from the octupolar crystal structure, and a correction term that accounts for the possible interactions (including the surface potential between the Al and TTB molecules), respectively.[14] The correction term includes possible changes in the electronic

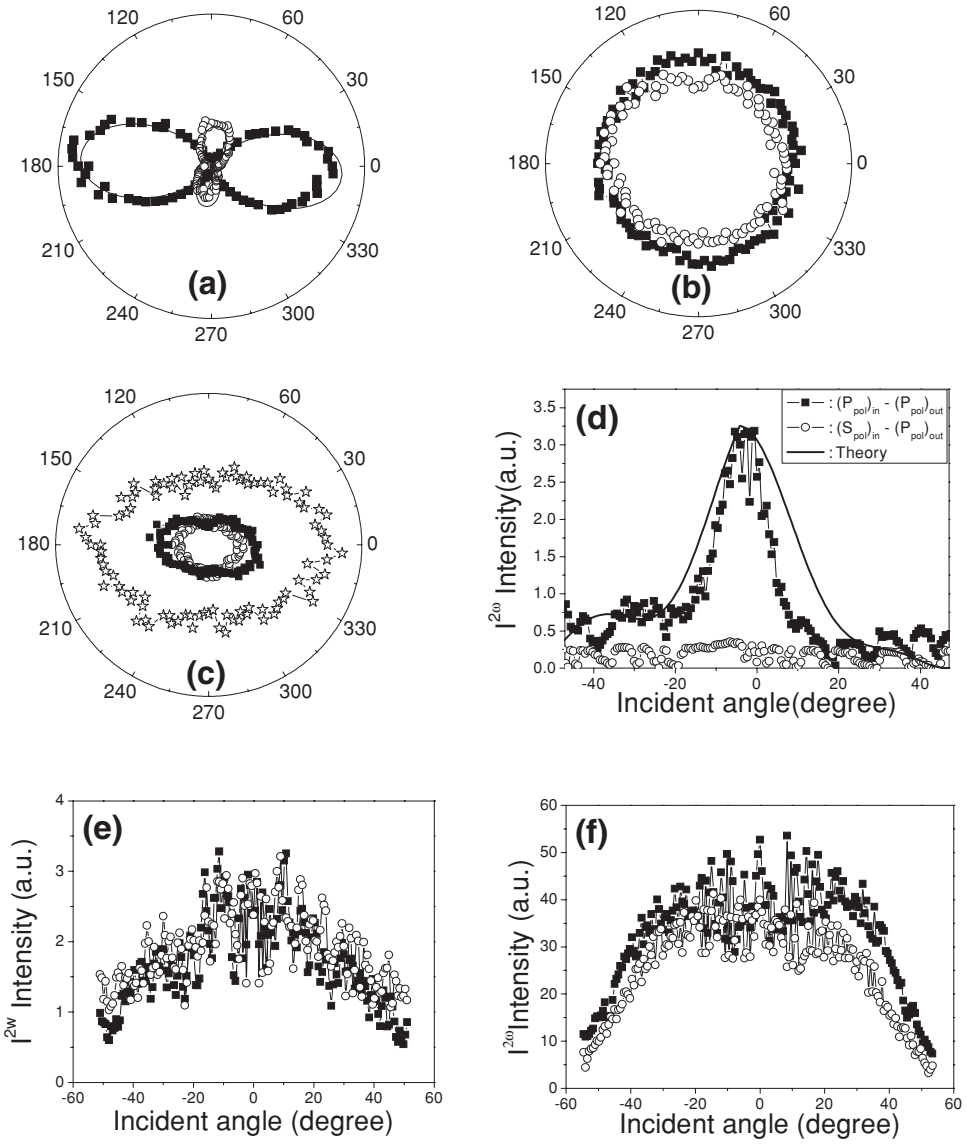

Figure 4. SHG polarization response, represented as polar diagrams, of a) cylinders on PI/ITO, b) polycrystals on PI/ITO, and c) polycrystals on Al/BK7 as a function of the incident polarization angle Φ. The solid squares, open circles, and open stars are the experimental data for $I_X(\Phi)$, $I_Y(\Phi)$, and $(I_X(\Phi) + I_Y(\Phi))$, respectively. Envelope fringes of d) cylinders on PI/ITO, polycrystals on e) PI/ITO and f) Al/BK7. The solid squares and open circles are the SHG intensity of the p- and s-polarization, respectively. The solid lines in (a) and (d) are the theoretically fitted curves. The Euler angles of the cylinder crystal are determined as (90°,90°,93°) from the polar plot and the Maker fringe experimental analysis.

properties of the molecules that are in contact with the metal, or possible modifications to the Al characteristics due to the presence of TTB molecules. In the present case, the sole Al/BK7 substrate excited with the same fundamental beam intensity level as the film produced no measurable signal. The metal substrate was damaged at a higher power level. We therefore conclude that the measured SHG efficiency originates primarily from an enhanced molecular response $I^{2\omega}{}_{INT}$ on the metal substrate.

To provide a refined measurement of the molecular orientation and the SHG efficiency in the cylinders and polycrystalline structures, we performed Maker Fringe-type experiments to explore the samples' SHG responses at various incidences. For this purpose the sample is rotated around the *Y*-axis by the angle θ (defined in Figure S2 in the Supporting Information), and the second harmonic is measured with an incident polarization along either the p-polarization or s-polarization direction. The size of the pump beam is about 150 μm; therefore, it illuminates only one cylinder on the sparse sample (Figure 1b), which is initially placed horizontally along the *Y*-direction. In the present case, the thickness of the films lies below the coherent length of the SHG process; thus, the "Maker" fringes should be considered to be "envelope" fringes representative of the coupling efficiency between the molecular orientation and the incident polarization direction.

For a quantitative comparison and determination of the Euler angle ψ, we calculated d_{eff},[1,15,16] which is the second-order

nonlinear optical coefficient of the TTB films. Assuming octupolar symmetry for the crystal domains (Figure S2b in the Supporting Information), d^2_{eff} can be expressed for the p-polarized input pump beam ω and the p-polarized output beam 2ω as:

$$d_{\text{eff}} = d_{11}[(S_1^2 - C_1^2)S_2 - 2(C_1 S_1)C_2] \tag{4a}$$

where $S_1 = \sin(\theta_2 + \psi)$, $\theta_2 = \sin^{-1}(\frac{1}{n_\omega}\sin\theta_1)$, $C_1 = \sqrt{1 - S_1^2}$, $S_2 = \sin(\theta_{2\omega} + \psi)$, $\theta_{2\omega} = \sin^{-1}(\frac{1}{n_{2\omega}}\sin\theta_1)$, and $C_2 = \sqrt{1 - S_2^2}$. For the normal incidence, $\theta = 0°$ and

$$d_{\text{eff}} = d_{11}[\sin\psi^3 - 3\sin\psi\cos\psi^2] \tag{4b}$$

This experimental condition corresponds to that of the polar plots, in which the d_{XXX}(of $I^{2\omega}{}_x(0,\Omega)$, Equation (3)) of the TTB molecules lie perpendicular to the (X,Y) plane and $\phi = 90°$. The corresponding experimental and fitted curve data for the cylinder sample are shown in Figure 4d. At normal incidence ($\theta = 0°$), the cylinder is placed so there is maximum coupling efficiency between the molecular orientation and the p-polarization, which we confirm by the high SHG intensity under p-polarization excitation, and the vanishing SHG under s-polarized excitation (Figure 4d). As the incident angle of the input fundamental beam is increased, the experimental data deviate somewhat from the fitted curve data and rapidly decrease for p-polarization; this is due to the loss of spatial overlap between the focal spot and the cylinder. However, it permits to confirm and measure the SHG efficiency and obtained with $\psi \approx 93°$. Figure 4e,f show the envelope fringes for the two polycrystals, one on PI/ITO (Figure 4e) and the other on Al/BK7 (Figure 4f). The SHG signal intensity is very large at a normal incidence, and as the incident angle of the pump beam increases, the signal decreases. Furthermore, when we consider the intensity with the birefringence results, each molecular plan for a microsized crystal is seen to lie perpendicular to the (X,Y) plane cylinder axis, or $\theta(Z,z) = 90°$, while ϕ and ψ are randomly oriented. The slightly different shape of the two curves in Figure 4b,c can be assigned to a slightly different disorder type in the sample plane.

In the case of the polycrystals, we assumed that both the crystal film and their substrate Al or PI are considered to be a nonlinear source material layer. The thicknesses used in the calculation are 990 μm, 3.35 μm, 1 μm, and 1.42 μm, for the quartz crystal, cylinders on PI/ITO, polycrystal on Al/BK7, and polycrystals on PI/ITO, respectively. The refractive indices at 532 and 1064 nm are 1.54690 and 1.53410 for quartz, respectively,[17] and 1.6720 and 1.5167 for the octupolar films, respectively.[18] The same refractive indices are used for the three films in the calculation. These refractive indices values have been determined by ellipsometry on thin films (USA, J. A. Woollam VUV-VASE UV-302).[19] The calculated second-order NLO coefficient, corrected for absorption effects, is found to be d_{11} = 20–35 pm V^{-1} [(47.7–83.6) × 10^{-9} esu] in the PI/ITO cylinder crystalline sample, assuming that the maximum coupling is achieved with $\psi = 93°$. This is a lower limit for two reasons; first, a higher ψ angle would lead to a higher nonlinear coefficient; and second, the sample contains empty spaces in the focal spot. Considering that the cylinder occupies only one tenth of the focal spot surface and the Gaussian repartition of the intensity on the focal spot, we conclude that the nonlinear coefficient of the cylinder is approximately 1000–1750 pm V^{-1} [(2387–4178) × 10^{-9}esu]. The value obtained after surface correction falls in the same range as the bulk TTB crystal value of $\|d\|$ = 1580 × 10^{-9}esu (662 pm V^{-1}), previously obtained with femtosecond pulses at 1028 nm.[1b] This confirms the crystalline nature of the cylinders. For the polycrystals grown on Al/BK7 and PI/ITO substrates, we obtain $d^{\text{eff}}{}_{11}$ values of 70–87 pm V^{-1} (167–208 × 10^{-9} esu) and 6.6 pm V^{-1} (15.8 × 10^{-9} esu), respectively. However, the effective nonlinear coefficient $d^{\text{eff}}{}_{11}$ does not originate from a purely coherent build-up of the nonlinearity in the sample. The much smaller $d^{\text{eff}}{}_{11}$ values of the polycrystals than the TTP crystal can be attributed to the incoherent construction of the signal from the polycrystals and a smaller dye concentration in the film composed of 20 wt% TTB in a PMMA matrix. Furthermore, the SHG remained the same for 1 year at room temperature and 3 days at 100 °C. The unusually large d_{11} value and high thermal stability indicate that cylinders are promising materials for SHG applications.

2.3. Electro-Optic Effect of Octupolar Patterned Films

We measured the EO properties of the films using a focused 633 nm HeNe laser beam with a diameter of approximately 200 μm.[20–22] Using the previous SHG measurement results for the symmetry and crystal direction on the substrate, we derived theoretical equations for the EO responses in octupolar crystals.[23]

The setup used for the EO measurements is depicted in Figure S4 (Supporting Information). The crystalline cylinder sample is placed between two electrodes and is illuminated at normal incidence in a propagation direction denoted by Z. The long axis of the cylinder is oriented in the X-direction, so that the octupolar molecules lie in the (Y,Z) plane. In this experimental coordinate configuration, the Euler angles (θ,ϕ) correspond to (90°,0°).

In an initial configuration, a half-wave plate ($\lambda/2$) placed before the sample and an analyzer placed after the sample are rotated simultaneously; this keeps the incoming and outgoing polarizations crossed. The other optical elements are fixed. The fast axis of the $\lambda/4$ plate is polarized along the Y-direction, and under this condition, the final output optical intensity, I_{out}, can be expressed as[23]

$$I_{\text{out}} = 2I_{\text{in}}\sin\beta^2\cos\beta^2(1 + \sin\Gamma) \tag{5}$$

where I_{in} is the incident intensity, β is the angle between the X-direction and the varying incoming polarization, Γ is the modulated phase shift between the two X and Y polarization components in the sample, with $\Gamma = \frac{2\pi}{\lambda}\Delta nL + \Gamma_{\text{m}}$, the modulated contribution $\Gamma_{\text{m}} = \frac{2\pi}{\lambda}n_{\text{m}}L$, and $n_{\text{m}} = \frac{1}{2}r_{11}E_{\text{m}}n_{\text{o}}^3$.

In a second possible configuration, the incident polarization is maintained at +45° and the analyzer is maintained at –45° relative to the X-direction. The $\lambda/4$ plate is rotated by the angle γ, which is defined by the angle between X and its fast axis (Figure S4 in the Supporting Information). Then the output intensity, I_{out}, is given by[23]

$$I_{out} = I_{in} \cdot \left[\frac{1}{2} \left[-\sin\frac{\Gamma}{2} + \cos\frac{\Gamma}{2} \left(\sin\gamma^2 - \cos\gamma^2 \right) \right]^2 + 2\sin\frac{\Gamma^2}{2} \sin\gamma^2 \cos\gamma^2 \right] \quad (6)$$

If the direction of the polarizer is +45° (β) relative to *X*, the slow axis of the quarter-wave plate is horizontal ($\gamma = 0°$), and the direction of the analyzer is –45° relative to X, then Equations (5) and (6) become equivalent:

$$I_{out}(E_m, \psi) = I_{in}\frac{1}{2}[1 + \sin\Gamma(E_m, \psi)] \quad (7)$$

with $\Gamma = \Gamma_0 + \Gamma_m$.

According to the SHG results described in Section 2.2 and our EO study,[23] the EO coefficient of the octupolar crystal system can be obtained using the preliminary Euler angles of octupolar molecules as determined by the SHG measurement. The detailed theoretical derivation is described in Jeong et al.[23] For a cylinder crystal with Euler angles ($\theta = 90°$, $\phi = 0°$, $\psi = 93°$), a π-modulated phase change in this configuration can be obtained using the half voltage $V_\pi = \sqrt{\frac{4\lambda L}{3r_{11}^2 n_o^5}}$. In both situations in which the incident light polarization $\theta = 45°$ and the Euler angles are (90°, 0°, 93°), the EO coefficient r_{11} of the cylinder crystal is deduced as[23]

$$r_{11} = \sqrt{\frac{4\lambda L}{3V_\pi^2 n_o^5}} \quad (8)$$

For the cylinder crystal which has Euler angles ($\theta = 90°$, $\phi = 0°$, $\psi = 0°$), we can obtain $V_\pi = \frac{\lambda}{r_{11} n_o^3}$ and the Y-axis component of the modulated refractive index, $n_Y(\psi) = n_0 - n_m$, with $n_m = \frac{1}{2} r_{11} E_m n_0^3$. Furthermore, the EO coefficient r_{11} of the cylinder crystal is deduced as[23]

$$r_{11} = \frac{\lambda}{V_\pi n_o^3} \quad (9)$$

In the case of polycrystals, the domains are expected to exhibit a random distribution at the micrometer size; therefore, Equation (8) cannot be applied. Instead, we assume that in Equation (7), $n_X(n_e) = n_Y(n_o)$ and $\sin\Gamma = \Gamma_m$ with $\Gamma \ll 1$; also, when the modulating electric field is 0, $I_{out} = I_{in}\frac{1}{2} = I_{DC}$. The effective EO coefficient $r_{eff} = r^{eff}_{11}$ can be derived as

$$r_{eff} = \sqrt{\frac{I_m \lambda L 4}{I_{DC} 3\pi V_m^2 n_0^5}} \quad (10)$$

It is generally assumed that the EO effect has a flat response ranging from DC to many hundreds of gigahertz.[24,25] But in a real system, the modulated EO signal intensity decreases by a factor of approximately four when the modulating electric field frequency is modified in the range of 1 to 5 kHz (**Figure 5**a). The EO signal is flat in the range of 5 to 11 kHz, increases to a local maximum near 13 kHz, and then decreases (Figure 5a,b). This frequency dependency implies the likely presence of other factors. It appears that at low frequencies, the modulation of the birefringence contributes to the modulation of the refractive index, in a manner similar to the EO response of domain dynamics in an $RbHSeO_4$ crystal[26] and the dipole reorientation behavior in a polymer matrix. A similar frequency-dependent behavior was observed in the cylinders and polycrystals. Hence, all EO coefficients of the samples were calculated at 4.0 kHz to minimize the birefringence contribution. Furthermore, the changes in the modulated light intensity I^{out}_m with the input beam polarization[23] (**Figure 6**b) and with the fast axis angle rotation of the $\lambda/4$ plate[23] (Figure 6c) showed excellent correlations with Equations (5) and (6), respectively. This confirms the validity of the analysis as outlined above.

However, the angle dependence of the modulated light intensity of the polycrystals that were measured while rotating the $\lambda/4$ plate (0° is the angle with the fast axis of $\lambda/4$ vertical) showed slightly different behavior depending on the substrate (Figure 6a,b). This can be attributed to the different domain patterns on each substrate, as observed in the SHG polarization and envelope fringe measurements (Figure 4b,c). For polycrystals on PI/ITO, the dependence of the modulated light intensity exhibits a symmetric feature pattern in both the vertical and horizontal directions of the fast axis of the quarter-wave plate, which means that the domains are randomly distributed. This

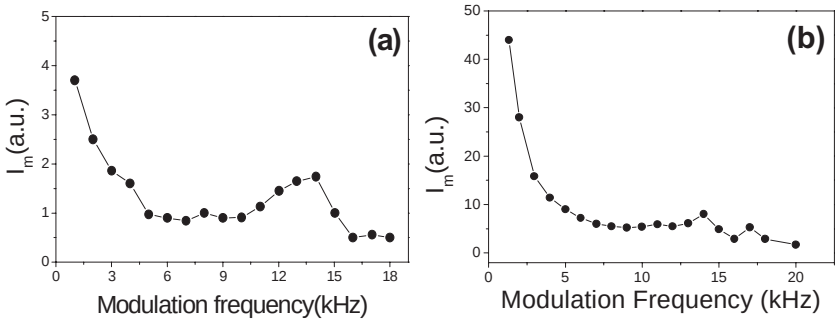

Figure 5. The frequency dependence of the electro-optic effect for the cylinders on a) PI/ITO and b) Al/BK7. The lines are guides for the eye.

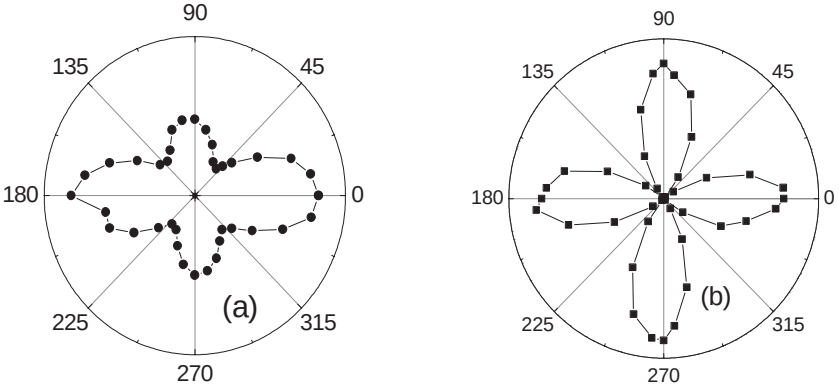

Figure 6. Plot of the modulated light intensity vs. fast axis angle of the $\lambda/4$ plate for the polycrystals on a) Al/BK7 and b) PI/ITO. The lines are guides for the eye.

is not the case for polycrystals on Al/BK7, since then the modulated light intensity is higher for the horizontal θ angle than for the vertical θ angle. The substrate may have induced a preferential orientation direction in the domains in the explored region, resulting in the remaining birefringence. This is also apparent in Figure 4c, in which the SHG polarization dependence exhibits a degree of anisotropy. However, these responses are allowed, evaluating the EO efficiency of the films, if we assume that the response originates from an effective nonlinear coefficient d_{11}^{eff} associated with an effective EO coefficient r_{11}^{eff}.

The EO coefficients were determined by applying the modulating electric field to the electrodes spaced by the dielectric spacer. The sample thickness was assumed to be the same as given above, and the refractive index was assumed to be 1.5825 at 633 nm.[18]

The EO coefficients for all the samples were calculated at a modulation frequency of 4 kHz. For the cylinder samples with $L = 3.35$ μm and Euler angles at (90°,0°,93°), we obtain the EO coefficient $r_{11} \approx 2300$ pm V^{-1} using the experimentally measured value of $V\pi = 230$ V combined with Equation (8). Also, in order to estimate the range of possible values of r_{11} for the sample with Euler angles (90°,0°,0°), we obtain an EO coefficient $r_{11} \approx 695$ pm V^{-1} using Equation (9).[23] Thus, for both cases $\psi \approx 0°$ and $\psi \approx 90°$, which makes r_{11} fall within the range $r_{11} \approx 695$–2300 pm V^{-1}. This range of values is consistent with the values of $d_{11} \approx 1000$–1750 pm V^{-1} [(2387–4178) $\times 10^{-9}$ esu] previously measured in the SHG results provided in Section 2.2, and with $d_{11} \approx 1000$–1500 pm V^{-1} found in similar samples.[15,16]

Using Equation (10), the EO coefficients for the polycrystals on Al/BK7 and PI/ITO were found to be $r^{eff}_{11} = 56.9$ pm V^{-1} and $r^{eff}_{11} = 12.2$ pm V^{-1}, respectively. These values are similar to what would be expected from the SHG measurement. Also similar to the SHG results, which result from metal enhancement effects, we observed that there is a more efficient EO response of the polycrystal on the Al/BK7 structure compared with the PI/ITO structure. Although there is scattering to a certain extent, these films have a very large nonlinear optical coefficient. The measured EO coefficients of the octupolar patterned films are large enough to satisfy application requirements.

3. Conclusions

We prepared thin films containing TTB in a PMMA matrix on Al/BK7 and PI/ITO substrates. The octupolar films contained both cylinders and polycrystals, and their characteristic crystallinity was confirmed by XRD and polarized microscopy measurements. The molecular crystal planes were oriented perpendicularly to the major cylinder axis, but were randomly oriented in the polycrystals. All samples exhibited large second order nonlinear and electro-optic coefficients, which originated from a coherent nonlinear effect in the cylinders. They were also due to the incoherent addition of nonlinear effects in the polycrystals, in which the response appeared to be enhanced by the metallic Al substrate. Due to their three-fold symmetry and lack of a ground state dipole moment, the nonlinear optical effect of the octupolar crystal films did not decrease over several months at room temperature, nor did they decrease in three days at 100 °C. The very large SHG coefficient ($d_{11} \approx 1000$–1750 pm V^{-1}), EO coefficient ($r_{11} \approx 695$–2300 pm V^{-1}), and high thermal stability of the cylinders are useful characteristics in second order nonlinear optic device applications.

4. Experimental Section

Preparation of Films: A 20 wt% TTB/PMMA film was prepared using a solution of TTB (0.2 g, 3×10^{-4} mol) and PMMA (MW = 100 000, 0.80 g) in chlorobenzene (17 mL). The solution was filtered with a 0.2 μm Teflon filter, and a few drops of the solution were placed on aluminum (200 Å)/glass (BK7) plates (≈λ/10) and polyimide (SE7492, 800Å)/ITO plates for crystals to grow. The Al and ITO layers were used as the electrodes for the EO measurements. The deposited plates were covered with glass caps on a vibration-free table and maintained for one week at ≈9–10 °C to evaporate the solvent. The film contained two distinct domains in a neighborhood on the substrate; one with polycrystals and the other with cylinders.

Measurement of Second Harmonic Generation: The pump beam was obtained from a 1064 nm Nd:YAG laser (10Hz, Q-switched, 7 ns pulse width). In the experimental setup, the laser beam passed through a polarizer, a λ/2 plate, and a high-pass filter before irradiating the film (Figure S2 in the Supporting Information). The beam polarization angle was varied by rotating the λ/2 plate in 3.2° increments using the step motor. Each SHG data point is an average of at least 30 measurements at 532 nm. To determine d_{11}, *Y*-cut quartz was used as a reference.

Measurement of Electro-Optic Coefficients: For the EO effects of the crystal films, a focused 633 nm He/Ne laser beam (beam size ≈ 200 μm) was employed. In the experimental setup shown in Figure S4 (Supporting Information), an incident beam was passed through an input linear polarizer, a λ/2 plate (to rotate the polarization of the input beam), a modulated crystal sample, a λ/4 plate, and an analyzer in a regular sequence.

In this configuration, the polarizer and the analyzer were always cross polarized. The EO coefficients were determined by applying the modulating electric field to the electrodes.

Supporting Information

Supporting Information is available from the Wiley Online Library or from the author.

Acknowledgements

This work was supported by a Korea Research Foundation Grant funded by the Korean Government (KRF-2008-313-C00348 and 2009-0068755), a National Research Foundation (NRF) grant (No. 2011-0020477), and the Priority Research Centers Program through the NRF funded by the Ministry of Education, Science and Technology (No. 2011-0018396).

Received: September 22, 2011
Published online: December 14, 2011

[1] a) M.-Y. Jeong, H. M. Kim, S.-J. Jeon, S. Brasselet, B. R. Cho, *Adv. Mater.* **2007**, *19*, 2107; b) V. Le Floc'h, S. Brasselet, J. Zyss, B. R. Cho, S. H. Lee, S.-J. Jeon, M. Cho, K. S. Min, M. P. Suh, *Adv. Mater.* **2005**, *17*, 196.
[2] M. J. Lee, M. Piao, M.-Y. Jeong, S. H. Lee, S.-J. Jeon, T. G. Lim, B. R. Cho, *J. Mater. Chem.* **2003**, *13*, 1030.
[3] H. C. Jeong, M. Piao, M.-Y. Jeong, K. M. Kang, G. Park, S.-J. Jeon, B. R. Cho, *Adv. Funct Mater.* **2004**, *14*, 64.

[4] C. Dhenaut, I. Ledoux, I. D. W. Samual, J. Zyss, M. Bourgault, H. Le Bozec, *Nature* **1995**, *374*, 339.
[5] V. R. Thalladi, S. Brasslet, H.-C. Weiss, D. Blaser, A. K. Katz, H. L. Carrell, R. Boese, J. Zyss, A. Nangia, G. R. Desiraju, *J. Am. Chem. Soc.* **1998**, *120*, 2563.
[6] S. Brasselet, J. Zyss, *J. Opt. Soc. Am. B.* **1998**, *15*, 257.
[7] J. Zyss, *J. Chem. Phys.* **1993**, *98*, 6583.
[8] J. Zyss, S. Brasselet, V. R. Thalladi, G. R. Desiraju, *J. Chem. Phys.* **1998**, 658.
[9] C. K. Chen, A. R. B. de Castro, Y. R. Shen, *Phys. Rev. Lett.* **1981**, *46*, 145.
[10] G. T. Boyd, Th. Rasing, J. R. R. Leite, Y. R. Shen, *Phys. Rev. B* **1984**, *30*, 519.
[11] S. V. Govorkov, N. I. Koroteev, I. L. Shumay, V. V. Yakovlev, *J. Opt. Soc. Am. B* **1991**, *8*, 1023.
[12] F. Charra, V. M. Agranovich, F. Kajzar, in *Organic Nanophotonics Mathematics, Physics and Chemistry*, Vol. *100*, (Eds: S. Brasselet, P. Gadenne. Anceau, J. Zyss), **2003**, p. 339.
[13] T. Manaka, M. Iwamoto, *Thin Solid Films* **2001**, *393*, 119.
[14] E. Itoh, H. Kokubo, S. Shouriki, M. Iwamoto, *J. Appl. Phys.* **1988**, *83*, 372.
[15] When equation 8 was published in ref. [1], there was a typing error in it.
[16] W. N. Herman, L. M. Hayden, *J. Opt. Soc. Am. B* **1995**, *12*, 416.
[17] CVI Laser Corporation optics catalog book (or www.cvimellesgriot.com/Company/Documentation.aspx/Index of Refraction (accessed June 2011).
[18] Vacuum UV Spectroscopic Ellipsometer measurement, USA, J. A. Woollam VUV- VASE UV-302. The Levenberg-Marquardt algorithm was used to obtain the best fit curves.
[19] a) H. G. Tompkins, W. A. McGahan, *Spectroscopic Ellipsometry and Reflectrometry*, Wiley Press, New York **1999**; b) A. Alvarez-Herrero, H. Guerrero, E. Bernabeu, D. Levy, *Appl. Opt.* **2002**, *41*, 6692.
[20] R. W. Boyd, *Nonlinear optics*, Academic Press, London **1992**.
[21] C. C. Teng, H. T. Man, *Appl. Phys. Lett.* **1990**, *56*, 1734.
[22] J. W. Wu, J. F. Valley, E. S. Binkley, J. T. Kenney, G. F. Lipscomb, R. Lytel, *Appl. Phys. Lett.* **1991**, *58*, 225.
[23] M. Y. Jeong, S. Brasselet, B. R. Cho, T. G. Lim, *Opt. Express* **2011**, *19*, 7979.
[24] D. S. Chemla, J. Zyss, *Nonlinear Optical Properties of Organic Molecules and Crystals*, Vol. 1, Academic Press, Orlando **1987**, Chap. II-8.
[25] R. G. Duncan, MS thesis, Virginia Polytechnic Institute and State University, **2002**.
[26] L. Guilbert, J. P. Salvestrini, M. D. Fontana, Z. Czapla, *Phys. Rev. B* **1998**, *58*, 2523.